GEOPHYSICS, VOL. 52, NO. 8 (AUGUST 1987); P. 1074–1084, 9 FIGS.

Accurate depth migration by a generalized phase-shift method

Dan Kosloff* and David Kessler*

ABSTRACT

A new depth migration method derived in the space-frequency domain is based on a generalized phase-shift method for the downward continuation of surface data. For a laterally variable velocity structure, the Fourier spatial components are no longer eigenvectors of the wave equation, and therefore a rigorous application of the phase-shift method would seem to require finding the eigenvectors by a matrix diagonalization at every depth step. However, a recently derived expansion technique enables phase-shift accuracy to be obtained without resorting to a costly matrix diagonalization. The new technique is applied to the migration of zero-offset time sections. As with the laterally uniform velocity case, the evanescent components of the solution need to be isolated and eliminated, in this case by the application of a spatially variant high-cut filter. Tests performed on the new method show that it is more accurate and efficient than standard integration techniques such as the Runge-Kutta method or the Taylor method.

INTRODUCTION

A basic part of seismic migration is the downward continuation of surface data to the subsurface. This downward continuation is carried out with some form of solution of a governing wave equation. In order to preserve the fidelity of the seismic data, it is desirable to have the downward continuation as accurate as possible. Gazdag (1978) and Bolondi et al. (1978) introduced the phase-shift method which yields complete accuracy for laterally uniform structures. However, when the velocity structure is laterally varying, all reported methods give only approximate results. They are not exact because they are either based on approximate solutions to the wave equation for the medium under consideration, or because they rely on discrete numerical-solution techniques such as finite differences (Claerbout and Doherty, 1972; Loewenthal et al., 1976).

This paper shows how the phase-shift method can be generalized to arbitrary velocity structures. The resulting technique at first appears cumbersome because it requires a matrix diagonalization in every depth step. However, Tal-Ezer (1984, 1986) and Tal-Ezer et al. (1986) indicate how the solution can be obtained accurately without resorting to the matrix diagonalization. The application of Tal-Ezer's method to depth migration results in a technique which is both accurate and efficient compared to methods based on a numerical solution of the wave equation. The new scheme is demonstrated for poststack migration.

In the next section, the generalized phase-shift method for an arbitrary velocity structure is derived. It is subsequently shown that for a laterally uniform velocity model the method degenerates into the ordinary phase-shift method as in Gazdag (1978) and Bolondi et al. (1978). Next we describe the implementation of the generalized phase-shift method with Tal-Ezer's solution technique. The resulting algorithm is tested for poststack migration of a synthetic time section obtained from a model with heterogeneous velocities.

THE GENERALIZED PHASE-SHIFT METHOD

The generalized phase-shift method is based on the solution of the temporally transformed acoustic wave equation

$$\frac{\partial^2 \tilde{P}}{\partial z^2} = -\frac{\omega^2}{c^2}\,\tilde{p} - \frac{\partial^2 \tilde{P}}{\partial x^2}, \tag{1}$$

where x and z, respectively, denote horizontal and vertical Cartesian coordinates, $\tilde{P}(x, z, \omega)$ denotes the temporal transform of the pressure field, ω is the frequency, and $c(x, z)$ is the velocity field (Kosloff and Baysal, 1983). As in Kosloff and Baysal (1983), it is convenient to recast equation (1) as a set of

Manuscript received by the Editor April 4, 1986; revised manuscript received January 26, 1987.
*Department of Geophysics and Planetary Sciences, Tel-Aviv University Ramat-Aviv, Tel-Aviv 69978, Israel.

two first-order coupled equations given by

$$\frac{\partial}{\partial z}\begin{bmatrix}\tilde{P}\\ \dfrac{\partial\tilde{P}}{\partial z}\end{bmatrix}=\begin{bmatrix}0 & 1\\ -\dfrac{\omega^2}{c^2}-\dfrac{\partial^2}{\partial x^2} & 0\end{bmatrix}\begin{bmatrix}\tilde{P}\\ \dfrac{\partial\tilde{P}}{\partial z}\end{bmatrix}. \tag{2}$$

The downward continuation in the migration consists of the solution (2) for each frequency at all depths under the initial conditions of the values of $\tilde{P}$ and $d\tilde{P}/dz$ at the earth's surface $z = 0$ (Kosloff and Baysal, 1983).

Since seismic data consist of time histories at discrete points on the earth's surface, the solution of equation (2) must include a discretization in the horizontal coordinate. With N_x denoting the number of seismic traces and dx the trace spacing, equation (2) transforms into a set of $2N_x$ coupled ordinary differential equations in the variables $\tilde{P}(idx, z, \omega)$ and $\partial\tilde{P}/\partial z(idx, z, \omega)$, $i = 0, \ldots, N_x - 1$. The horizontal discretization requires an approximation for the derivative term in equation (2). Whether this derivative is calculated by the Fourier method as with the ordinary phase-shift method (Gazdag, 1978), or by finite differences with periodic horizontal boundary conditions, it can be written as the cyclic convolution

$$\frac{\partial^2\tilde{P}}{\partial x^2}(idx, z, \omega)=\sum_{j=0}^{N_x}\tilde{P}(jdx, z, \omega)W_{i-j}, \tag{3}$$

where W_i denotes a convolutional operator (for nonperiodic boundary conditions, the convolution becomes noncyclic). For example, for second-order finite differences, $W_0 = -2/dx^2$ and $W_{-1} = W_1 = 1/dx^2$, and $W_i = 0$ for $|i| \geq 2$. For the Fourier second-derivative operator,

$$W_0 = -\left(\frac{2\pi}{N_x dx}\right)^2\frac{L(L+1)}{3}$$

and (4)

$$W_n=\frac{1}{2}\left(\frac{2\pi}{N_x\,dx}\right)^2(-1)^n\frac{\cos\left(\dfrac{\pi n}{N_x}\right)}{\sin^2\left(\dfrac{\pi n}{N_x}\right)},\qquad n\neq 0,$$

with $N_x = 2L + 1$ (see the Appendix). In most reported applications, the derivative has been calculated with the fast Fourier transform (FFT) (Gazdag, 1978; Stolt, 1978; Gazdag, 1980; Kosloff and Baysal, 1983); however, a direct application of equation (4) gives identical results. Computational efficiency determines which approach is used in the calculations.

With the spatial discretization and specification of the second-derivative approximation, equation (2) can be recast as

$$\frac{\partial}{\partial z}\begin{bmatrix}\tilde{P}\\ \dfrac{\partial\tilde{P}}{\partial z}\end{bmatrix}=\begin{bmatrix}\underline{\mathbf{A}}\end{bmatrix}\begin{bmatrix}\tilde{P}\\ \dfrac{\partial\tilde{P}}{\partial z}\end{bmatrix}. \tag{5}$$

$$\begin{bmatrix}\tilde{P}\\ \dfrac{\partial\tilde{P}}{\partial z}\end{bmatrix}$$

denotes a column vector of length $2N_x$ containing first the N_x pressures $P(idx, z, \omega)$ and then the N_x pressure derivatives $\partial\tilde{P}/\partial z(idx, z, \omega)$, $i = 0, \ldots, N_x - 1$. The $2N_x$ by $2N_x$ matrix $\underline{\mathbf{A}}$ can be partitioned according to

$$\begin{bmatrix}\underline{\mathbf{A}}\end{bmatrix}=\begin{bmatrix}0 & I_{N_x}\\ A_{21} & 0\end{bmatrix},$$

where I_{N_x} denotes the N_x by N_x identity matrix, and the elements of the N_x by N_x symmetric submatrix A_{21} are given by

$$\begin{bmatrix}A_{21}\end{bmatrix}=\begin{bmatrix}\dfrac{-\omega^2}{c_1^2}-W_0 & -W_1 & \cdots & -W_{N_x-1}\\ -W_1 & \dfrac{-\omega^2}{c_2^2}-W_0 & \cdots & -W_{N_x-2}\\ \cdot & \cdot & \cdots & \cdot\\ -W_{N_x-1} & \cdot & \cdots & \dfrac{-\omega^2}{c_{N_x}^2}-W_0\end{bmatrix}. \tag{6}$$

In equation (6), c_i is a shorthand notation for $c(idx, z)$, and we used the periodicity of the coefficients W_i given by $W_{-i} = W_{N_x-i}$. As with the ordinary phase-shift method, the solution here is propagated in depth increments. Within each increment z to $z + dz$, the velocity is assumed to be invariant in the vertical direction although it may vary horizontally. The solution of equation (5) can then be written as

$$\begin{bmatrix}\tilde{P}\\ \dfrac{\partial\tilde{P}}{\partial z}\end{bmatrix}_{z+dz}=\exp\left[Ad_z\right]\begin{bmatrix}\tilde{P}\\ \dfrac{\partial\tilde{P}}{\partial z}\end{bmatrix}_{z}. \tag{7}$$

We now show that solution (7), excluding evanescent components, embodies a phase shift of eigenvector coefficients of $\underline{\mathbf{A}}$. For periodic boundary conditions and a symmetric second-derivative operator, the N_x by N_x submatrix A_{21} in equation (6) is symmetric. Its eigenvalues are therefore real. We denote these eigenvalues by $\lambda_0, \lambda_1, \ldots, \lambda_{N_x-1}$ and the corresponding normalized and mutually orthogonal eigenvectors by $\mathbf{V}_0, \mathbf{V}_1, \ldots, \mathbf{V}_{N_x-1}$. For simplicity, we assume that all the eigenvalues are nonzero (which is usually the case in actual calculations); however, the derivations can be modified to account for zero eigenvalues as well. Given the eigenvalues and eigenvectors of A_{21}, it can be verified by substitution that the $2N_x$ eigenvalues of matrix $\underline{\mathbf{A}}$ are given by $\pm\sqrt{\lambda_i}$, $i = 0, \ldots, N_x - 1$. The corresponding eigenvectors are given by

$$\begin{bmatrix}\mathbf{V}_0\\ \sqrt{\lambda_0}\mathbf{V}_0\end{bmatrix},\quad\begin{bmatrix}\mathbf{V}_1\\ \sqrt{\lambda_1}\mathbf{V}_1\end{bmatrix},\ldots,\begin{bmatrix}\mathbf{V}_{N_x-1}\\ \sqrt{\lambda_{N_x-1}}\mathbf{V}_{N_x-1}\end{bmatrix},$$

$$\begin{bmatrix}\mathbf{V}_0\\ -\sqrt{\lambda_0}\mathbf{V}_0\end{bmatrix}\cdots\begin{bmatrix}\mathbf{V}_{N_x-1}\\ -\sqrt{\lambda_{N_x-1}}\mathbf{V}_{N_x-1}\end{bmatrix}.$$

With these eigenvectors we define a $2N_x$ by $2N_x$ matrix $\mathbf{Q}$ in which the columns consist of the eigenvectors of $\underline{\mathbf{A}}$. We then

have the relation

$$Q^{-1}AQ = \underline{\Lambda}, \tag{8}$$

where $\underline{\Lambda}$ is the diagonal matrix

$$\underline{\Lambda} = \begin{bmatrix} \sqrt{\lambda_0} & & & & 0 \\ & \sqrt{\lambda_1} & & & \\ & & \ddots & & \\ & & & -\sqrt{\lambda_0} & \\ 0 & & & & \ddots \\ & & & & -\sqrt{\lambda_{N_x-1}} \end{bmatrix} \tag{9}$$

and

$$Q^{-1} = \frac{1}{\sqrt{2}} \begin{bmatrix} \mathbf{V}_0^T & \cdots & \dfrac{\mathbf{V}_0^T}{\sqrt{\lambda_0}} \\ \mathbf{V}_1^T & \cdots & \dfrac{\mathbf{V}_1^T}{\sqrt{\lambda_1}} \\ \cdot & \cdots & \cdot \\ \mathbf{V}_{N_x-1}^T & \cdots & \dfrac{\mathbf{V}_{N_x-1}^T}{\sqrt{\lambda_{N_x-1}}} \end{bmatrix}. \tag{10}$$

When both sides of equation (7) are multiplied by $\underset{\sim}{Q}$ from the left, we obtain [using equations (8), (9), and (10)],

$$Q^{-1} \begin{bmatrix} \tilde{P} \\ \dfrac{\partial \tilde{P}}{\partial z} \end{bmatrix}_{z+dz} = \exp\,[\Lambda\, dz] Q^{-1} \begin{bmatrix} \tilde{P} \\ \dfrac{\partial \tilde{P}}{\partial z} \end{bmatrix}_z. \tag{11}$$

The entries of the diagonal matrix exp $[\Lambda\, dz]$ are given by

$$\left[e^{\Lambda dz}\right] = \begin{bmatrix} e^{\sqrt{\lambda_0}\,dz} & & & & 0 \\ & e^{\sqrt{\lambda_1}\,dz} & & & \\ & & \ddots & & \\ & & & e^{-\sqrt{\lambda_0}dz} & \\ 0 & & & & \ddots \\ & & & & e^{-\sqrt{\lambda_{N_x-1}}\,dz} \end{bmatrix}. \tag{12}$$

The phase-shift character of the downward extrapolation now becomes apparent. The vectors

$$Q^{-1} \begin{bmatrix} \tilde{P} \\ \dfrac{\partial \tilde{P}}{\partial z} \end{bmatrix}_z \quad \text{and} \quad Q^{-1} \begin{bmatrix} \tilde{P} \\ \dfrac{\partial \tilde{P}}{\partial z} \end{bmatrix}_{z+dz}$$

give the coefficients of the eigenvector expansion of

$$\begin{bmatrix} \tilde{P} \\ \dfrac{\partial \tilde{P}}{\partial z} \end{bmatrix}_z \quad \text{and} \quad \begin{bmatrix} \tilde{P} \\ \dfrac{\partial \tilde{P}}{\partial z} \end{bmatrix}_{z+dz},$$

respectively. In the propagation of the solution from depth z to depth $z + dz$, the components are multiplied according to equations (11) and (12) by exp $(\sqrt{\lambda_i}\,dz)$ or exp $(-\sqrt{\lambda_i}\,dz)$, $i = 0, \ldots, N_x - 1$, respectively. The $2N_x$ eigenvalues of matrix $\underline{\Lambda}$, given by $\pm\sqrt{\lambda_i}$, $i = 0, \ldots, N_x - 1$, are either purely real or purely imaginary depending upon the sign of λ_i. When an eigenvalue $\pm\sqrt{\lambda_i}$ is imaginary, the corresponding coefficient is propagated in equation (11) by a phase shift. Conversely, when $\pm\sqrt{\lambda_i}$ is real, the component is propagated by a multiplication by a real exponential. As with the ordinary phase-shift method, the components in this case span the evanescent part of the solution. For numerical stability (as discussed later), the evanescent components need to be eliminated from the solution.

SOLUTION FOR HORIZONTALLY UNIFORM STRUCTURES

In this section we show that with the Fourier second-derivative approximation and for horizontally uniform structures, the phase-shift relation (11) degenerates into a variant of the ordinary phase-shift method described in Gazdag (1978).

Denote the uniform velocity in a strip between z and $z + dz$ by c_0. The elements of the submatrix A_{21} in equation (6) are now

$$\left[A_{21}\right]_{ij} = -\frac{\omega^2}{c_0^2}\,\delta_{ij} - W_{i-j}, \qquad i,j = 0, \ldots, N_x - 1, \tag{13}$$

where W_i is given by equation (4). For the Fourier method second-derivative approximation, the eigenvalues and eigenvectors of equation (13) can be calculated. From the Appendix, the values $1/\sqrt{N_x}\,(e^{iK_\nu jdx})$, $\nu = 0, \ldots, N_x - 1$ [or equivalently, cos $(K_\nu jdx)$ and sin $(K_\nu jdx)$ if one wishes to deal with real eigenvectors] represent the components of the νth eigenvector of the operator W. By equation (13), they also represent the components of the νth eigenvector of A_{21}. K_ν is given by

$$K_\nu = \begin{cases} \dfrac{2\pi}{N_x dx}\,\nu & \text{for } \nu = 0, \ldots, \dfrac{N_x}{2} - 1 \\ -\dfrac{2\pi}{N_x dx}\,(N_x - \nu) & \text{for } \nu = \dfrac{N_x}{2}, \ldots, N_x - 1 \end{cases}. \tag{14}$$

The corresponding eigenvalues are given by

$$\lambda_\nu = -\frac{\omega^2}{c^2} + K_\nu^2. \tag{15}$$

The entries of the N_x by N_x matrix $\underset{\sim}{V}$, composed from the eigenvectors of $[A_{21}]$, are then given by

$$V_{jr} = \frac{1}{\sqrt{N_x}} \exp\left(i\,\frac{2\pi}{N_x}\,jr\right), \qquad j, r = 0, \ldots, N_x - 1.$$

This matrix is exactly the discrete Fourier transform (DFT) matrix (e.g., Bracewell, 1978). When it operates on a vector, the result is the discrete spatial Fourier transform of that

vector. The matrix $\underline{\mathbf{Q}}$ of equation (10) then becomes

$$\left[Q^{-1}\right]=\frac{1}{\sqrt{2}}\begin{bmatrix} V^*_{00} & \cdots & V^*_{0\,N_x-1} & \frac{i\omega}{c_0}V^*_{00} & \cdots & \frac{i\omega}{c_0}V^*_{0\,N_x-1} \\ V^*_{10} & \cdots & V^*_{1\,N_x-1} & i\eta_1 V^*_{10} & \cdots & i\eta_1 V^*_{1\,N_x-1} \\ \cdot & \cdots & \cdot & \cdot & \cdots & \cdot \\ V^*_{N_x-1\,0} & \cdots & V^*_{N_x-1\,N_x-1} & i\eta_{N_x-1}V^*_{N_x-1\,0} & \cdots & i\eta_{N_x-1}V^*_{N_x-1\,N_x-1} \\ V^*_{00} & \cdots & V^*_{0\,N_x-1} & \frac{-i\omega}{c_0}V^*_{00} & \cdots & \frac{-i\omega}{c_0}V^*_{0\,N_x-1} \\ V^*_{10} & \cdots & V^*_{1\,N_x-1} & -i\eta_1 V^*_{10} & \cdots & -i\eta_1 V^*_{1\,N_x-1} \\ \cdot & \cdots & \cdot & \cdot & \cdots & \cdot \\ V^*_{N_x-1\,0} & \cdots & V^*_{N_x-1\,N_x-1} & -i\eta_{N_x-1}V^*_{N_x-1\,0} & \cdots & -i\eta_{N_x-1}V^*_{N_x-1\,N_x-1} \end{bmatrix}, \tag{16}$$

where

$$\eta_r=\sqrt{\frac{\omega^2}{c_0^2}-K_r^2},\quad r=0,\ldots,N_x-1 \qquad \text{and} \qquad V^*_{k\ell}=\frac{1}{\sqrt{N_x}}\exp\left[-i\frac{2\pi}{N_x}k\ell\right].$$

With this result, the propagated solution (11) now becomes

$$\begin{bmatrix} \tilde{\tilde{P}}_0+i\eta_0\frac{\partial\tilde{\tilde{P}}_0}{\partial z} \\ \vdots \\ \tilde{\tilde{P}}_{N_x-1}+i\eta_{N_x-1}\frac{\partial\tilde{\tilde{P}}_{N_x-1}}{\partial z} \\ \tilde{\tilde{P}}_0-i\eta_0\frac{\partial\tilde{\tilde{P}}_0}{\partial z} \\ \vdots \\ \tilde{\tilde{P}}_{N_x-1}-i\eta_{N_x-1}\frac{\partial\tilde{\tilde{P}}_{N_x-1}}{\partial z} \end{bmatrix}_{z+dz} = \begin{bmatrix} e^{i\eta_0\,dZ_0} & & & & & \\ & \ddots & & & & \\ & & e^{i\eta_{N_x-1}\,dz_0} & & & \\ & & & e^{-i\eta_0\,dZ_0} & & \\ & & & & \ddots & \\ & & & & & e^{-i\eta_{N-x-1}\,dZ_0} \end{bmatrix} \begin{bmatrix} \tilde{\tilde{P}}_0+i\eta_0\frac{\partial\tilde{\tilde{P}}_0}{\partial z} \\ \vdots \\ \tilde{\tilde{P}}_{N_x-1}+i\eta_{N_x-1}\frac{\partial\tilde{\tilde{P}}_{N_x-1}}{\partial z} \\ \tilde{\tilde{P}}_0-i\eta_0\frac{\partial\tilde{\tilde{P}}_0}{\partial z} \\ \vdots \\ \tilde{\tilde{P}}_{N_x-1}-i\eta_{N_x-1}\frac{\partial\tilde{\tilde{P}}_{N_x-1}}{\partial z} \end{bmatrix}_z, \tag{17}$$

where $\tilde{\tilde{P}}$ denotes the spatial Fourier transform of $\tilde{P}$,

$$\tilde{\tilde{P}}(r,z,\omega)=\frac{1}{\sqrt{N_x}}\sum_{n=0}^{N_x-1}\tilde{P}(ndx,z,\omega)\exp\left[-i\frac{\pi}{N_x}n\nu\right].$$

It is now clear that equation (17) is a variant of the ordinary phase-shift method of Gazdag (1978) and Bolondi et al. (1978). With the z coordinate increasing downward, the components $\tilde{\tilde{P}}_\nu+(i\eta_\nu)(\partial\tilde{\tilde{P}}_\nu/\partial z)$, $\nu=0,\ldots,N_x-1$, correspond to upgoing waves, and $\tilde{\tilde{P}}_\nu-(i\eta_\nu)(\partial\tilde{\tilde{P}}/\partial z)$, $\nu=0,\ldots,N_{x-1}$ correspond to downgoing waves. As pointed out in Kosloff and Baysal (1983), this variant of the phase-shift method assures the continuity of both $\tilde{\tilde{P}}$ and $\partial\tilde{\tilde{P}}/\partial z$ across horizontal interfaces. This is unlike the phase-shift migration method in Gazdag (1978) which includes only upgoing energy and does not assure the continuity of $\partial\tilde{\tilde{P}}/\partial z$. From a practical viewpoint, however, it is doubtful whether assuring the continuity of $\partial\tilde{\tilde{P}}/\partial z$ lends any advantages to poststack migration. The exploding-reflector concept on which the migration is based includes only upgoing energy (Loewenthal et al., 1976) and therefore does not account accurately for amplitudes.

SOLUTION FOR ARBITRARY VELOCITY STRUCTURES

When the velocity structure varies arbitrarily in the lateral direction, the eigenvalues and eigenvectors of matrix $\underline{\mathbf{A}}$ can no longer be obtained by inspection. It would therefore seem that a matrix diagonalization would have to be performed before each propagation according to equation (11). However, recent work by Tal-Ezer (1984, 1986) and Tal-Ezer et al. (1986) indicates how the generalized phase-shift method can be effected without having to resort to expensive matrix diagonalizations. This section describes the implementation of Tal-Ezer's method to depth migration. A more detailed discussion of the solution technique can be found in Tal-Ezer (1984, 1986) and Tal-Ezer et al. (1986).

The solution is based on a Chebychev expansion of the generalized phase-shift method before matrix diagonalization (7). The expansion is derived from the scalar expansion for the function e^x given by

$$e^x=\sum_{k=0}^{\infty}C_kJ_k(R)Q_k\left(\frac{x}{R}\right),\qquad |x|<R \tag{18}$$

(e.g., Hamming, 1973). J_k denotes the kth-order Bessel function, Q_k denote Chebychev polynomials, $C_0=1$ and $C_k=2$ for $k>0$, and x is real (or at least in sufficient proximity to the real axis). When x is imaginary (or sufficiently close to the imaginary axis), the above expansion is replaced by the series

$$e^x=\sum_{k=0}^{\infty}C_kJ_k(R)T_k\left(\frac{x}{R}\right),\qquad |x|<R, \tag{19}$$

where the polynomials $T_k(x)$ satisfy the recurrence relations

$$T_0(x) = 1,$$

$$T_1(x) = x,$$

and (20)

$$T_{k+1}(x) = T_{k-1}(x) + 2xT_k(x)$$

(Tal-Ezer, 1984, 1986). By analogy with equation (19), the exponent in equation (7) is expanded according to

$$\begin{bmatrix} \tilde{P} \\ \dfrac{\partial \tilde{P}}{\partial z} \end{bmatrix}_{z+dz} = \exp\,[A\,dz] \begin{bmatrix} \tilde{P} \\ \dfrac{\partial \tilde{P}}{\partial z} \end{bmatrix}_z = \sum_{k=0}^{\infty} J_k(R) C_k T_k\left(\frac{Adz}{R}\right) \begin{bmatrix} \tilde{P} \\ \dfrac{\partial \tilde{P}}{\partial z} \end{bmatrix}_z. \quad (21)$$

This expansion is valid when the eigenvalues of $[Adz]$ are purely imaginary. As discussed in the next section, this requires elimination of the evanescent components from the solution. Also, R must be chosen large enough to span the range of the eigenvalues of $[Adz]$. It was shown in Tal-Ezer (1984) that for $k > R$, the series expansion converges exponentially. The number of terms required in the sum in equation (21) will therefore always be finite.

Equation (21) serves as the basis for implementing the generalized phase-shift migration. First the range **R** of the eigenvalues of $[Adz]$ needs to be estimated (but not necessarily evaluated exactly). Based on the case of laterally uniform velocity, we have found the estimate $R = \omega dz/c_{\min}$, with $c_{\min}$ denoting the lowest velocity in the strip $(z, z + dz)$, sufficient for stable results. The Bessel functions $J_k(R)$ are computed next. The solution

$$\begin{bmatrix} \tilde{P} \\ \dfrac{\partial \tilde{P}}{\partial z} \end{bmatrix}_{z+dz}$$

is then calculated recursively according to the following:

(a) Given

$$T_{k-1} \begin{bmatrix} \tilde{P} \\ \dfrac{\partial \tilde{P}}{\partial z} \end{bmatrix}_z$$

and

$$T_k \begin{bmatrix} \tilde{P} \\ \dfrac{\partial \tilde{P}}{\partial z} \end{bmatrix}_z,$$

generate the next polynomial by the formula

$$T_{k+1} \begin{bmatrix} \tilde{P} \\ \dfrac{\partial \tilde{P}}{\partial z} \end{bmatrix}_z = T_{k-1} \begin{bmatrix} \tilde{P} \\ \dfrac{\partial \tilde{P}}{\partial z} \end{bmatrix}_z + 2\begin{bmatrix} Adz \\ \overline{R} \end{bmatrix} \begin{bmatrix} \tilde{P} \\ \dfrac{\partial \tilde{P}}{\partial z} \end{bmatrix}_z; \quad (22)$$

(b) add another term to the sum in equation (21).

The first two values of T_0, T_1 needed to initialize the recursion are given by

$$T_0 \begin{bmatrix} \tilde{P} \\ \dfrac{\partial \tilde{P}}{\partial z} \end{bmatrix}_z = \begin{bmatrix} \tilde{P} \\ \dfrac{\partial \tilde{P}}{\partial z} \end{bmatrix}_z$$

and

$$T_1 \begin{bmatrix} \tilde{P} \\ \dfrac{\partial \tilde{P}}{\partial z} \end{bmatrix}_z = \begin{bmatrix} Adz \\ \overline{R} \end{bmatrix} \begin{bmatrix} \tilde{P} \\ \dfrac{\partial \tilde{P}}{\partial z} \end{bmatrix}_z$$

(Tal-Ezer, 1984, 1986). Steps (a) and (b) are repeated until a sufficient number of terms have been calculated in the sum (21). Then the solution is carried out in the next lower level. When $\tilde{P}(x, z, \omega)$ has been calculated completely, the final migrated section is cumulated by

$$P_{\text{mig}}(x, z) = \sum_{\omega} \tilde{P}(x, z, \omega)$$

(Kosloff and Baysal, 1983).

ELIMINATION OF EVANESCENT ENERGY

The real eigenvectors of the solution to the wave equation (2) correspond to evanescent components. These are nonsinusoidal inhomogeneous waves. They can be generated, for instance, when crossing velocity interfaces at angles beyond the critical angle, or from seismic sources that generate spherical waves (Aki and Richards, 1980). Since evanescent components decay exponentially with distance, the information contained in them is usually lost and they therefore cannot be used in seismic imaging. The evanescent components can lead to numerical instability in the form of exponential growth of rounding errors. Consequently, depth migration based on depth extrapolation with the full acoustic wave equation requires the elimination of the evanescent energy (Kosloff and Baysal, 1983).

Figure 1 shows the location of the eigenvalues of matrix $\underline{\mathbf{A}}$ of equation (7) in the complex plane. In an ideal solution, evanescent components corresponding to the real eigenvalues would be eliminated, whereas components corresponding to the imaginary eigenvalues would be unaltered. Unfortunately, in the general case this requires the separation of the evanescent components through a costly matrix diagonalization. A method for eliminating the evanescent components without the matrix diagonalization and without severely affecting the nonevanescent components is therefore required.

A scheme proposed in Kosloff and Baysal (1983) included use of the Fourier method and elimination of all the Fourier components whose wavenumbers satisfy $K_x > \omega/c_{\max}$, where $c_{\max}$ denotes the highest velocity in the depth increment between z and $z + dz$. Although this scheme has proven stable, it can also eliminate steeply dipping events in low-velocity regions.

In this study we examined the alternative of applying a zero-phase, spatially variant, high-cut filter to $\tilde{P}$ and $\partial\tilde{P}/\partial z$ after each step of the propagation of the solution, according to equation (21). The high-cut wavenumber for the filter K_{cut} at each point of application was based on the criterion $K_{\text{cut}} = \omega/c_{\max}$, where $c_{\max}$ denotes the highest velocity in a taper

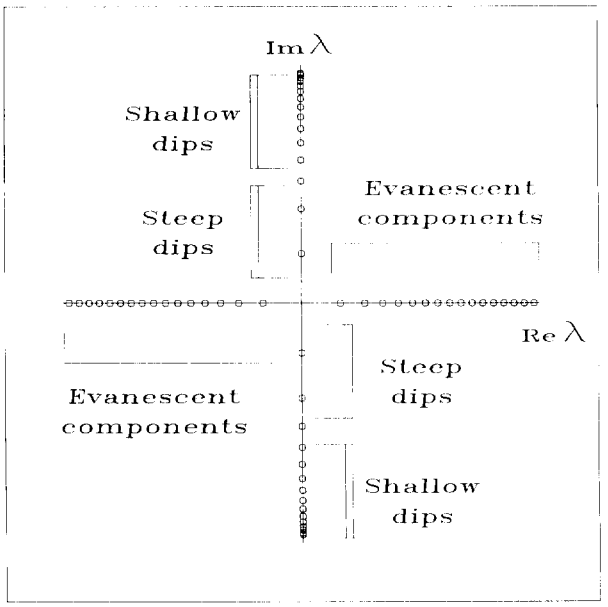

FIG. 1. Eigenvalues of matrix $\underline{A}$ in the complex plane.

region surrounding the point of application. In the present study the region size was chosen to be 12 traces. The total length of the filter was 41 points.

The following synthetic example illustrates the removal of the evanescent energy. The structure consisted of four layers with dips ranging between 0 and approximately 70 degrees (Figure 2). The velocity structure of the model included two regions of velocities 1500 m/s and 3000 m/s separated by a vertical interface (Figure 2). This example, though highly artificial, serves the purpose of showing the important characteristics of evanescent energy removal.

The synthetic zero-offset time section for this model is shown in Figure 3. The section contains 160 traces and 128 time samples. The section was calculated by *f-k* modeling (Stolt, 1978) (the model was constructed to make all energy travel through region 1 to allow the section to be obtained with modeling based on uniform velocity). The result of applying the generalized phase-shift migration with a spatially variant evanescent filter is shown in Figure 4. We have found that fairly long filters are required for obtaining satisfactory results, and in the present example the filter contained 41 coefficients. As Figure 4 shows, all events were reproduced correctly. For comparison, in Figure 5 we show the result of migration with removal of the evanescent energy by the FFT, as in Kosloff and Baysal (1983). In Figure 5, the steeply dipping events are not reproduced because the removal of the evanescent energy had to be based on the high velocity in region 2.

PRACTICAL ASPECTS OF APPLYING THE GENERALIZED PHASE-SHIFT METHOD

In this section we discuss a few factors relevant to efficient implementation of the generalized phase-shift method.

Kosloff and Baysal (1983) pointed out that poststack depth migration by depth extrapolation should include upgoing energy only. However, use of the full acoustic wave equation can cause the generation of downgoing energy at sharp velocity interfaces (Kosloff and Baysal, 1983). The solution was to remove the downgoing waves from the final section by filtering out all negative wavenumbers. In the present study, we chose instead to use a modified version of the full acoustic wave equation which is impedance-matched for waves impinging vertically on horizontal interfaces (Baysal et al., 1984).

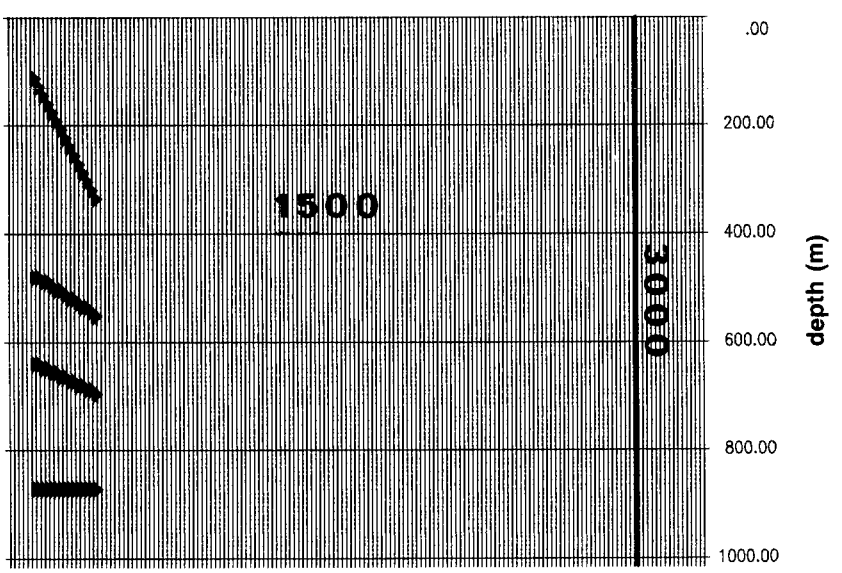

FIG. 2. Depth structure of four dipping layers with dips ranging between 0 and 70 degrees.

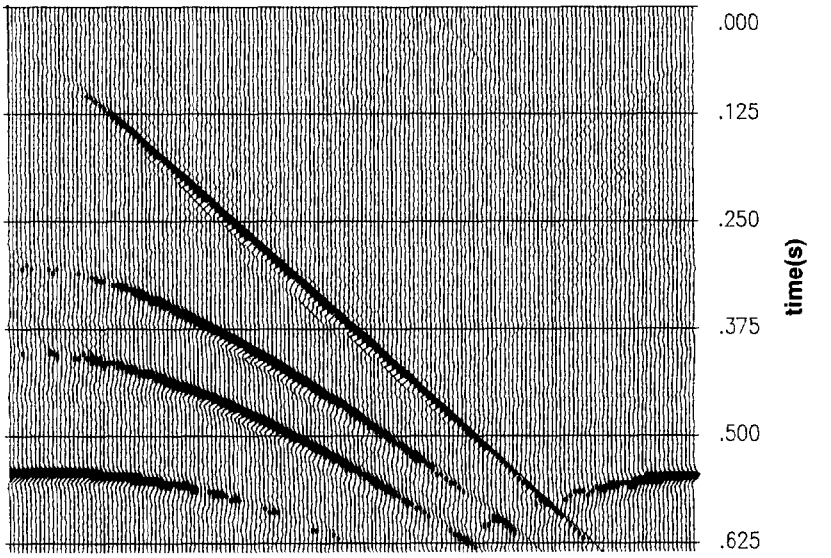

FIG. 3. Zero-offset time section corresponding to Figure 2.

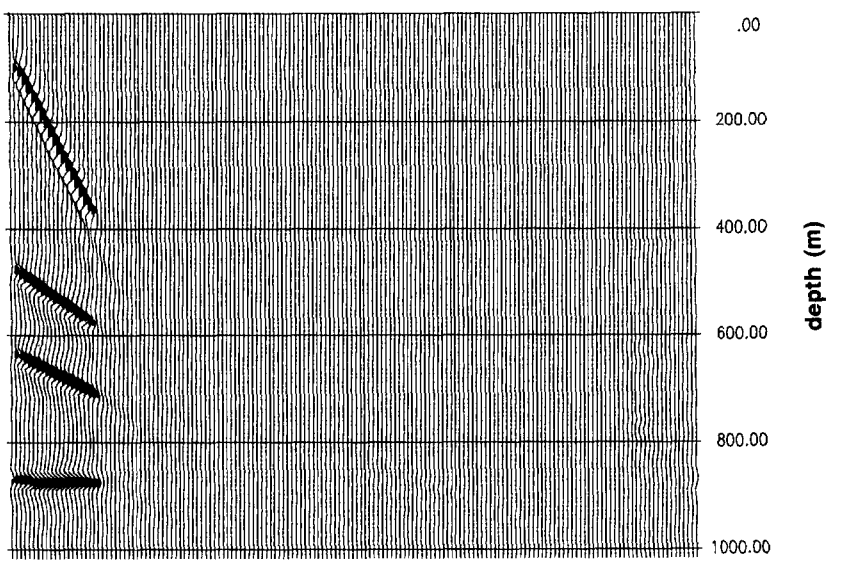

FIG. 4. Migrated section using the spatially variant evanescent filter.

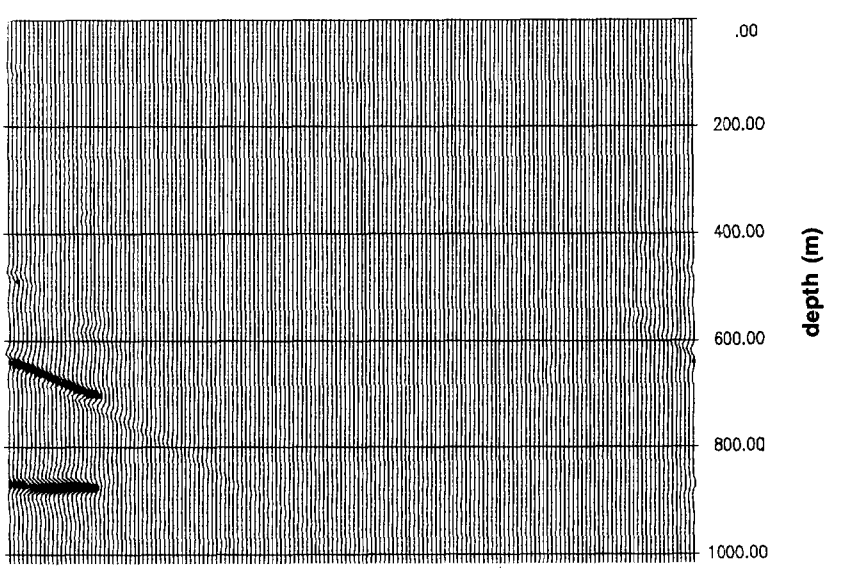

FIG. 5. Migrated section using the FFT filter.

With this wave equation, the system (2) is replaced by

$$\frac{\partial}{\partial z}\begin{bmatrix}\tilde{P}\\ c\dfrac{\partial\tilde{P}}{\partial z}\end{bmatrix}=\begin{bmatrix}0 & \dfrac{1}{c}\\ c\left(\dfrac{\omega^2}{c^2}-\dfrac{\partial^2}{\partial x^2}\right) & 0\end{bmatrix}\begin{bmatrix}\tilde{P}\\ c\dfrac{\partial\tilde{P}}{\partial z}\end{bmatrix}. \tag{23}$$

The basic variables are now $\tilde{P}$ and $c(\partial\tilde{P}/\partial z)$. Since the final imaged section is given by

$$P_{\text{mig}}(x, z)=\sum_{\omega}\tilde{P}(x, z, \omega)$$

(Kosloff and Baysal, 1983), only the real parts of $\tilde{P}$ and $c(\partial\tilde{P}/\partial z)$ need to be used in the calculations. This results in a savings of a factor of two in computational effort compared to the previous scheme.

The next question is when the series expansion by Tal-Ezer's method can be safely truncated. Since the Chebychev polynomials in equation (19) are bounded by unity, the magnitude of the Bessel coefficients can serve as a criterion for truncating the expansion (Tal-Ezer, 1984). Since the Bessel functions $J_k(R)$ tend to zero exponentially for $k > R$ (Tal-Ezer, 1984), we adopted the strategy of truncating the series at a k value for which the magnitude of $J_k(R)$ becomes insignificant compared to the magnitude of the largest coefficient found so far.

The next issue concerns choice of the depth step dz for the migration. From an economic point of view, Tal-Ezer's method is most efficient for large steps. However, sampling considerations dictate small steps (e.g., $dz \approx cdt/2$ with dt equal to the time sampling rate and c equal to a characteristic interval velocity). A slight modification of equation (21), however, can allow propagation in large depth steps while also obtaining results at intermediate levels:

$$\begin{aligned}\begin{bmatrix}\tilde{P}\\ \dfrac{\partial\tilde{P}}{\partial z}\end{bmatrix}_{z+\alpha dz} &= \exp\,[A\alpha\, dz]\begin{bmatrix}\tilde{P}\\ \dfrac{\partial\tilde{P}}{\partial z}\end{bmatrix}_{z}\\ &=\sum_{k=0}^{\infty}J_k(\alpha R)C_k\,T_k\left(\frac{Adz}{R}\right)\begin{bmatrix}\tilde{P}\\ \dfrac{\partial\tilde{P}}{\partial z}\end{bmatrix}_{z},\end{aligned} \tag{24}$$

with $0 < \alpha \leq 1$. In equation (24), the Chebychev matrix polynomials T_k obtained in equation (22) are also used for the intermediate levels, and only additional sets of Bessel functions $J_k(\alpha R)$ need to be evaluated (a relatively inexpensive calculation). The size of the depth step is therefore determined by the degree of discretization required for the velocity field. Propagation through large homogeneous regions (e.g., the ocean layer) can be carried out in one step.

Finally, we compare the efficiencies of the generalized phase-shift method and methods based on standard techniques for solving ordinary differential equations. We considered the simplified system

$$\frac{\partial}{\partial z}\begin{bmatrix}\tilde{P}\\ \dfrac{\partial\tilde{P}}{\partial z}\end{bmatrix}=\begin{bmatrix}0 & 1\\ -\dfrac{\omega^2}{c^2} & 0\end{bmatrix}\begin{bmatrix}\tilde{P}\\ \dfrac{\partial\tilde{P}}{\partial z}\end{bmatrix}, \tag{25}$$

obtained from equation (2) by assuming uniform velocity and setting the spatial derivative term to zero. With initial conditions $\tilde{P} = 1$ and $\partial\tilde{P}/\partial z = 0$, the exact solution of this system is $\tilde{P} = \cos(\omega z/c)$ and $\partial\tilde{P}/\partial z = -(\omega/c)\sin(\omega z/c)$. The range $\mathbf{R}$ of the eigenvalues of equation (25) is given by $\mathbf{R} = \omega/c$. We compared the computational effort for solving this equation for different interval sizes $\omega z/c$ using Tal-Ezer's method, a fourth-order Runge-Kutta method (Kosloff and Baysal, 1983), and a third-order Taylor method (Gazdag, 1980; Berkhout and Van Wulften, 1979). In the comparison we required machine accuracy (32 bit) for the generalized phase-shift method, and examined the performance of the other two methods for, respectively, 1 percent and 0.1 percent accuracy. The results of the comparison are summarized in Figure 6 in which the horizontal axis gives the step size and the vertical axis gives the number of required function evaluations (e.g., the number of multiplications by the matrix $\underline{\mathbf{A}}$).

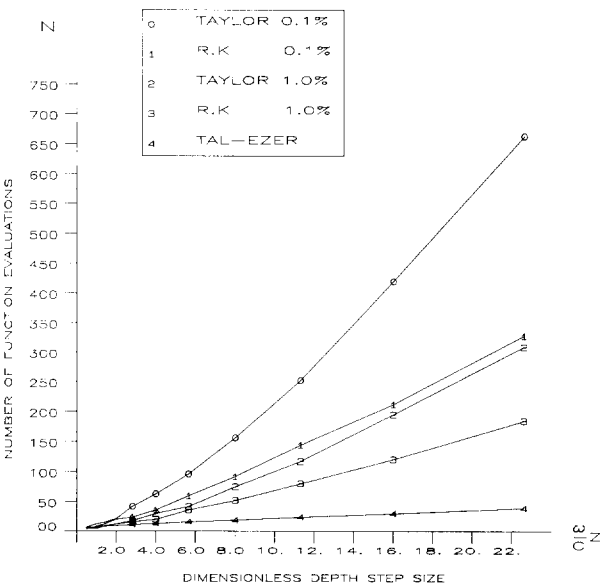

FIG. 6. Comparison of Taylor, Runge-Kutta, and Tal-Ezer methods.

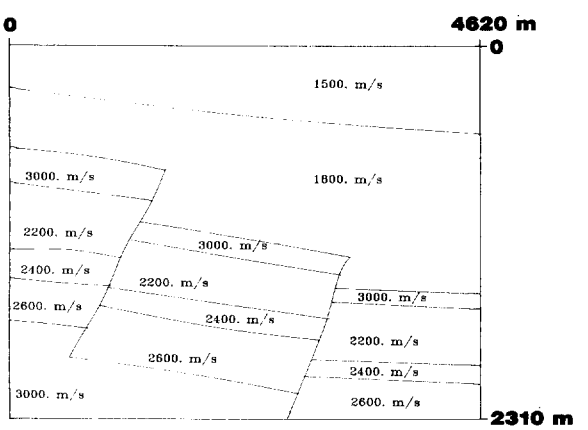

FIG. 7. Depth structure for the heterogeneous model.

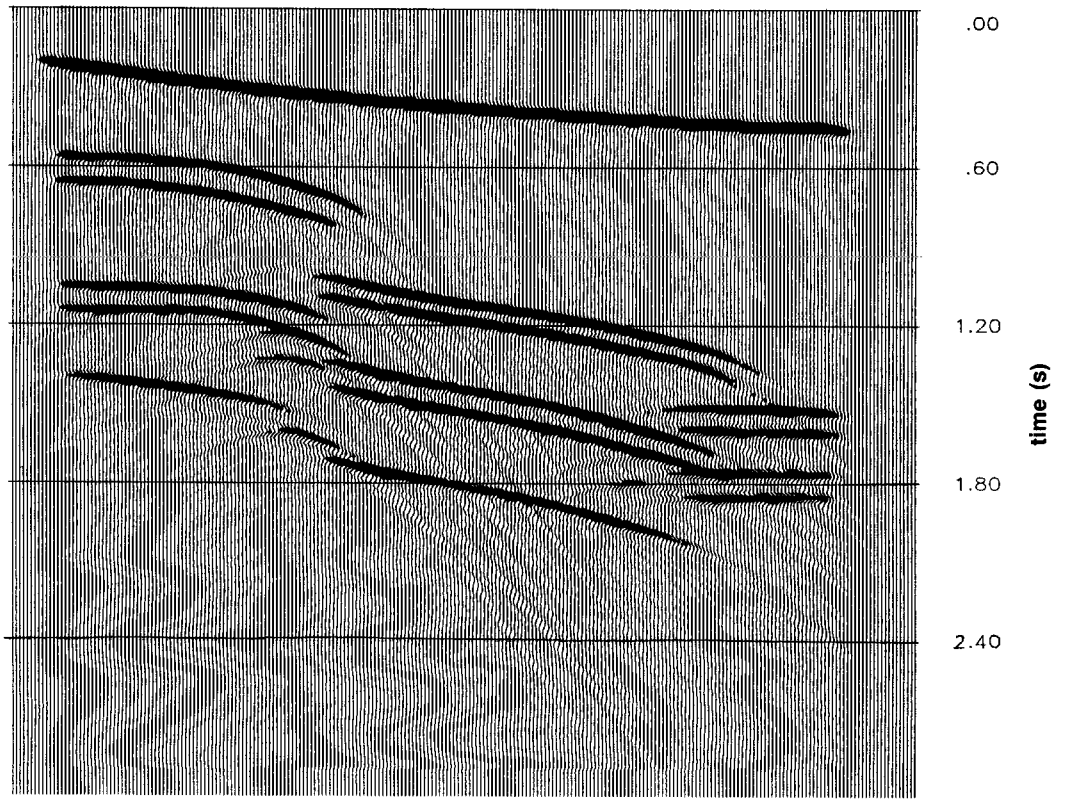

FIG. 8. Zero-offset time section corresponding to Figure 7.

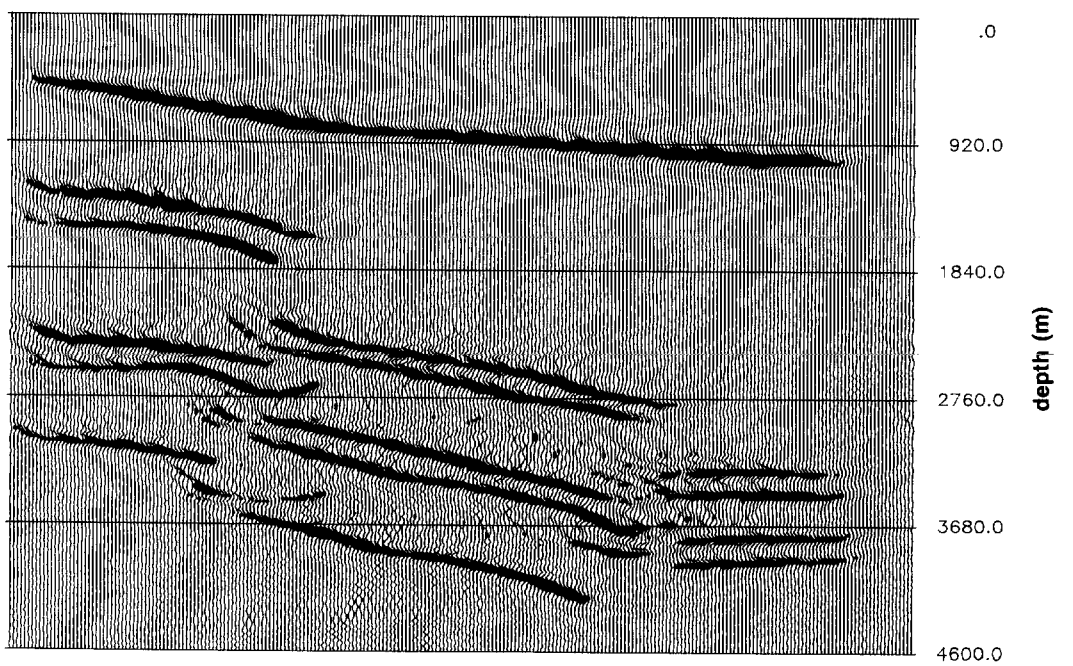

FIG. 9. Migrated section by the generalized phase-shift method.

The results show the distinct superiority of Tal-Ezer's method over the Runge-Kutta and Taylor methods. In contrast to the Runge-Kutta method and the Taylor method, the relative efficiency of Tal-Ezer's technique improves with an increase in increment size. The ratio $N/(\omega z/c)$ then approaches an asymptotic value of unity (Tal-Ezer 1984, 1986). Conversely, because of the accumulation of errors in each step, the relative efficiencies of the Runge-Kutta method and the Taylor method decrease for large distances. This indicates that extreme caution must be exercised in the choice of integration steps when using these methods since, even with a step size well below the stability limit, the quality of the results at large depths can be severely degraded. In addition to its superior performance, Tal-Ezer's method has the additional benefits of machine accuracy and continuous error control.

EXAMPLE: FAULTED STRUCTURE

In this section we present an example of migration of a synthetic time section obtained from a highly heterogeneous, faulted model (Figure 7). The model contains a number of velocity regions which are broken by two faults. The horizontal velocity contrast across the faults reaches a factor of 1:2 in certain locations (Figure 7).

The synthetic zero-offset time section obtained from the model is shown in Figure 8. The section was produced by the Fourier forward-modeling algorithm described in Kosloff and Baysal (1982). An exploding-reflector option was applied for producing the zero-offset section (Loewenthal et al., 1976). The calculation used a grid size of 231 × 231 with horizontal and vertical grid spacings of 20 m and 10 m, respectively. In order to reduce multiple energy, the nonreflecting two-way wave equation described in Baysal et al. (1984) was used. It is important to emphasize that the time section and the migration were produced by different methods.

Figure 9 shows the result of applying the generalized phase-shift depth migration to the time section. The migration used the correct interval velocities of the model (this is seldom the case with field data), so all events migrated to their correct locations. The faults are well-defined, except for what appears as overmigration at the truncations of the layers. This overmigration probably can be attributed to the fact that the velocity changes there by a factor of two within one trace spacing.

CONCLUSIONS

An accurate depth migration technique has been presented which is based on an expansion of the formal solution to the acoustic wave equation. The new algorithm is faster and also more accurate than methods based on standard techniques for solving ordinary differential equations, such as the Runge-Kutta method or the Taylor method.

Depth migration by depth extrapolation with the full acoustic wave equation requires removal of evanescent energy when the structure is not laterally uniform. In this study the evanescent energy was eliminated by applying a spatially variant, high-cut filter to the solution after each step. The filter coefficients were adjusted to match the velocity in a window around the point of application. The synthetic example suggests that the procedure may be successful even in situations of highly varying velocity.

We believe that the techniques used in this study can be applied to other areas of geophysics that require the solution of large systems of coupled linear differential equations. In particular, the method of Tal-Ezer has already been applied to seismic forward modeling by the Fourier method (Tal-Ezer et al., 1986), as well as to common-shot migration (Reshef and Kosloff, 1986).

REFERENCES

Aki, K., and Richards, P. G., 1980, Quantitative seismology, theory and methods: W. H. Freeman and Co.

Baysal, E., Kosloff, D., and Sherwood J. W. C., 1984, A two-way nonreflecting wave equation: Geophysics, **49**, 132–141.

Berkhout, A. J., and Van Wulften Palthe, D. W., 1979, Migration in terms of spatial deconvolution: Geophys. Prosp., **27**, 261–291.

Bolondi, G., Rocca, F., and Savelli, S., 1978, A frequency-domain approach to two-dimensional migration: Geophys. Prosp., **26**, 750–772.

Bracewell, R. N., 1978, The Fourier transform and its applications: McGraw-Hill Book Co., Inc.

Claerbout, J. F., and Doherty S. M., 1972, Downward continuation of moveout-corrected seismograms: Geophysics, **37**, 741–768.

Gazdag, J., 1978, Wave-equation migration with the phase-shift method: Geophysics, **43**, 1342–1351.

——— 1980, Wave-equation migration with the accurate space derivative method: Geophys. Prosp., **28**, 60–70.

Hamming, R. W., 1973, Numerical methods for scientists and engineers: McGraw-Hill Book Co., Inc.

Kosloff, D., and Baysal, E., 1982, Forward modeling by a Fourier method: Geophysics, **47**, 1402–1412.

——— 1983, Migration with the full acoustic wave equation: Geophysics, **48**, 677–687.

Loewenthal, D., Lu, L., Roberson R., and Sherwood, J. W. C., 1976, The wave equation applied to migration: Geophys. Prosp., **24**, 380–399.

Reshef, M., and Kosloff, D., 1986, Migration of common shot gathers: Geophysics, **51**, 324–331.

Stolt, R. H., 1978, Migration by Fourier transform: Geophysics, **43**, 23–48.

Tel-Ezer, 1984, Ph.D. thesis, Tel-Aviv Univ.

——— 1986, Spectral methods in time for hyperbolic problems: Soc. Industr. Appl. Math., J. Numer. Anal., **23**, 11–20.

Tal-Ezer, H., Kosloff, D., and Koren, Z., 1986, An accurate scheme for seismic forward modeling: Geophys. Prosp., in press.

APPENDIX

In this appendix we derive the weights of the Fourier second-derivative operator. Let $f(n)$ represent a discrete function defined over the spatial grid points $n = 0, \ldots, N_x - 1$. The following derivations assume that the number of points Nx is odd (this avoids special consideration of the Nyquist frequency which only exists for even-numbered grids). The forward and the inverse discrete Fourier transforms (DFT) of $f(n)$ are defined by

$$\tilde{f}(\nu) = \sum_{n=0}^{N_x-1} f(n) \exp\left[-i\frac{2\pi}{N_x}\nu n\right], \qquad \nu = -L, \ldots, 0, \ldots, L, \qquad \text{(A-1)}$$

and

$$f(n) = \frac{1}{N_x} \sum_{\nu=-L}^{L} \tilde{f}(\nu) \exp\left[i \frac{2\pi}{N_x} \nu n\right], \quad n = 0, \ldots, N_x - 1, \tag{A-2}$$

with $N_x = 2L + 1$ (Bracewell, 1978). The Fourier second-derivative approximation is obtained by multiplying $\tilde{f}(\nu)$ by $-(2\pi\nu/N_x dx)^2$ for $\nu = -L, \ldots, 0, \ldots, L$, and forming the inverse transform. This gives

$$\frac{d^2 f}{dx^2}(n) = \frac{1}{N_x} \sum_{\nu=-L}^{L} -\left(\frac{2\pi\nu}{N_x dx}\right)^2 \tilde{f}(\nu) \exp\left[i \frac{2\pi}{N_x} \nu n\right] \tag{A-3}$$

or, by substituting $\tilde{f}(\nu)$ from equation (A-1),

$$\frac{d^2 f}{dx^2}(n) = \frac{1}{N_x} \sum_{\nu=-L}^{L} -\left(\frac{2\pi\nu}{N_x dx}\right)^2 \times \exp\left[i \frac{2\pi}{N_x} \nu n\right] \left\{ \sum_{n'=0}^{N_x-1} f(n') \exp\left[-i \frac{2\pi}{N_x} \nu n'\right] \right\}.$$

Changing the order of the summation and combining terms yields

$$\frac{d^2 f}{dx^2}(n) = \frac{1}{N_x} \sum_{n'=0}^{N_x-1} f(n') \times \sum_{\nu=-L}^{L} -\left(\frac{2\pi\nu}{N_x dx}\right)^2 \exp\left[i \frac{2\pi}{N_x} (n - n')\nu\right]. \tag{A-4}$$

Equation (A-3) expresses a convolution of the form

$$\frac{d^2 f}{dx^2}(n) = \mathbf{W} * \mathbf{f}, \tag{A-5}$$

with W_n given by

$$W_n = \frac{1}{N_x} \sum_{\nu=-L}^{L} -\left(\frac{2\pi\nu}{N_x dx}\right)^2 \exp\left[i \frac{2\pi}{N_x} \nu n\right]. \tag{A-6}$$

Equation (A-6) can be expressed as the limit

$$W_n = \frac{1}{N_x dx^2} \lim_{\alpha \to n} \frac{d^2}{d\alpha^2} \left\{ \sum_{\nu=-L}^{L} \exp\left[i \frac{2\pi}{N_x} \alpha_\nu\right] \right\}.$$

This equation can be evaluated directly by taking the second derivative of the geometrical series sum formula and then passing to the limit $\alpha \to n$. The final result becomes

$$W_0 = -\left(\frac{2\pi}{N_x dx}\right)^2 \frac{L(L+1)}{3},$$

and

$$W_n = \frac{1}{2}\left(\frac{2\pi}{N_x dx}\right)^2 (-1)^n \frac{\cos\left(\frac{\pi n}{N_x}\right)}{\sin^2\left(\frac{\pi n}{N_x}\right)}, \quad n \neq 0.$$